Modeling biological oscillations: integration of short reaction pauses into a stationary model of a negative feedback loop generates sustained long oscillations

Louis Yang, Ming Yang

Sustained oscillations are frequently observed in biological systems consisting of a negative feedback loop, but a mathematical model with two ordinary differential equations (ODE) that has a negative feedback loop structure fails to produce sustained oscillations. Only when a time delay is introduced into the system by expanding to a three-ODE model, transforming to a two-DDE model, or introducing a bistable trigger do stable oscillations present themselves. In this study, we propose another mechanism for producing sustained oscillations based on periodic reaction pauses of chemical reactions in a negative feedback system. We model the oscillatory system behavior by allowing the coefficients in the two-ODE model to be periodic functions of time – called pulsate functions – to account for reactions with go-stop pulses. We find that replacing coefficients in the two-ODE system with pulsate functions with micro-scale (several seconds) pauses can produce stable system-wide oscillations that have periods of approximately one to several hours long. We also compare our two-ODE and three-ODE models with the two-DDE, three-ODE, and three-DDE models without the pulsate functions. Our numerical experiments suggest that sustained long oscillations in biological systems with a negative feedback loop may be an intrinsic property arising from the slow diffusion-based pulsate behavior of biochemical reactions.

PeerJ PrePrints

PeerJ PrePrints | https://dx.doi.org/10.7287/peerj.preprints.1272v1 | CC-BY 4.0 Open Access | rec: 29 Jul 2015, publ: 29 Jul 2015

Modeling biological oscillations: integration of short reaction pauses into a stationary model of a negative feedback loop generates sustained long oscillations

ABSTRACT

Sustained oscillations are frequently observed in biological systems consisting of a negative feedback loop, but a mathematical model with two ordinary differential equations (ODE) that has a negative feedback loop structure fails to produce sustained oscillations. Only when a time delay is introduced into the system by expanding to a three-ODE model, transforming to a two-DDE model, or introducing a bistable trigger do stable oscillations present themselves. In this study, we propose another mechanism for producing sustained oscillations based on periodic reaction pauses of chemical reactions in a negative feedback system. We model the oscillatory system behavior by allowing the coefficients in the two-ODE model to be periodic functions of time – called pulsate functions – to account for reactions with go-stop pulses. We find that replacing coefficients in the two-ODE system with pulsate functions with micro-scale (several seconds) pauses can produce stable system-wide oscillations that have periods of approximately one to several hours long. We also compare our two-ODE and three-ODE models with the two-DDE, three-ODE, and three-DDE models without the pulsate functions. Our numerical experiments suggest that sustained long oscillations in biological systems with a negative feedback loop may be an intrinsic property arising from the slow diffusion-based pulsate behavior of biochemical reactions.

Louis Z. Yang[1] and Ming Yang[2]

[1]The Wharton School, University of Pennsylvania, 3620 Locust Walk, Suite 2400, Philadelphia, PA 19104, USA

[2]Department of Botany, Oklahoma State University, 301 Physical Sciences, Stillwater, OK 74078, USA

Corresponding author: Ming Yang, Department of Botany, Oklahoma State University, 301 Physical Sciences, Stillwater, OK 74078; telephone: 405-744-9508; email address: ming.yang@okstate.edu

INTRODUCTION

Oscillations are a prevalent phenomenon occurring at multiple levels in living organisms. Understanding the basic mechanism for generating oscillations in living organisms is fundamentally important to understanding the basic principles in biology. Currently, how oscillations in living organisms are generated is not well understood. A key to understanding such a mechanism is to identifying underlying causes of sustained oscillation in simple biological systems.

Mathematical models have indicated that a negative feedback loop is required but not sufficient for generating sustained oscillations (Ferrell, Tsai and Yang, 2011; Harima et al., 2014). Mathematical modeling with ordinary differential equations (ODE) revealed that only when a negative feedback loop is coupled with either a delayed action along the feedback loop (Ferrell, Tsai and Yang, 2011; Harima et al., 2014) or another positive feedback loop (Ferrell, Tsai and Yang, 2011), can sustained oscillations be generated. In essence, adding more components to a feedback loop such as a positive feedback loop is mathematically equivalent to delaying an action in the negative feedback loop. In a simple biological oscillating system, such as the oscillation of Hes7 protein in mice, it does not involve an additional feedback loop other than the auto-repression of *Hes7* transcription by the direct binding of Hes7 to its own promoter (Bessho et al., 2003). Furthermore, deletions of the introns of the *Hes7* gene shorten the oscillation period, but do not abolish the oscillation, indicating the robustness of the oscillation (Takashima et al., 2011; Harima et al., 2013). It is also striking that the periods of the oscillations of Hes7 and its homolog Hes1 are similar, i.e. 2-3 hours, even though the two proteins are expressed in different cells (Harima et al., 2014). Oscillations with similar durations, which fall under the definition of ultradian rhythm, have also been observed in other biological processes such as adrenal corticosterone secretion in animals (Tapp, Holaday and Natelson, 1984; Engler et al., 1989; Jasper and Engeland, 1991) and humans (Weitzman et al., 1971), and the signal transduction in the EGF-stimulated ERK/MAPK pathway (Albeck, Mills and Brugge, 2013). These oscillations are likely the fastest in systems of large biomolecules.

The above mentioned studies of Hes7 suggest that the processing of the *Hes7* transcript precursor to the mature intronless form of the *Hes7* mRNA causes a delay in the negative feedback loop. However, if all the steps in the negative feedback loop are continuous processes, any delay due to differential reaction rates between two consecutive steps will be temporary as each reaction step will adjust its output based on the input from the previous step in a closed negative feedback loop. This argues that one or more steps in the negative feedback loop need to be discrete in order to produce a sustained oscillation.

Discreteness of biochemical reactions is likely a general phenomenon. Frequent pauses with durations from nearly a millisecond to seconds were observed in an in vitro enzymatic reaction involving a single enzyme molecule (Yang et al., 2003). Frequent pauses with durations from 1-6 seconds were also observed in an in vitro RNA transcriptional process (Neuman et al., 2003). Pauses with similar durations have also been observed in two independent in vitro microtubule assembly experiments (Kerssemakers et al., 2006; Schek et al., 2007). The reaction pauses have been proposed to be a diffusion-based phenomenon, although one proposal was developed on the basis of subdiffusion within the enzyme molecule (Kou and Xie, 2004) and the other on the basis of slow diffusion of a reactant to the reaction site in biological systems (Yang, 2014). If so, slow diffusion can, in general, cause the same kind of pauses in *in vivo* biochemical reactions since the

PeerJ PrePrints | https://dx.doi.org/10.7287/peerj.preprints.1272v1 | CC-BY 4.0 Open Access | rec: 29 Jul 2015, publ: 29 Jul 2015

diffusion coefficients in cellular compartments are small and the spatial confinement of the reactions requires at least some of the reactants to diffuse to the reaction centers. In this report, we propose that slow diffusion-based short reaction pauses can generate long oscillations in a two-ODE model of a simple negative feedback loop. Our model produces robust sustained oscillations with periods in the range of hours when the periods of molecular reactions and pauses are in the range of seconds that conform to the pauses observed in aforementioned molecular reactions. The periods and peak heights of the oscillations can also be increased with the addition of a third component in a three-ODE model. Thus, our model provides an explanation to how hours-long oscillations can be generated from a physical constraint in a negative feedback loop of biochemical reactions.

METHODS

The two-ODE and three-ODE models described in (Ferrell, Tsai and Yang, 2011) were used as the basic forms of our models while the original parameters α and β were replaced with a pulsate function in our models. The pulsate function was derived by Fourier analysis, which is based on the assumption that *in vivo* biochemical reactions in general undergo periodic pauses due to the slow diffusion rates relative to the chemical reaction rates. The numerical experiments were conducted, and Figs. 2-6 and Figs. A.1 and A.2 were initially generated, in MATLAB using the ODE solver ode45. Fig. 1 was drawn in PowerPoint. All figures were modified and assembled in Adobe Photoshop CS2.

RESULTS AND DISCUSSION

The non-oscillatory two-ODE model

Mathematical models have been proposed to describe oscillations of proteins during the cell cycle (Ferrell, Tsai and Yang, 2011). These models are based on a basic two-ODE form as illustrated by Eqs. [1] and [2], where x and y are two arbitrary chemicals in a negative feedback loop. Here x is activated through some exogeneous mechanism which in turn activates y. Then, the increasing level of y deactivates x. This type of negative feedback loop model is a simple representation of a wide variety of oscillatory systems. The α_1 term in Eq. [1] represents the activation of chemical x (which is assumed to be a simple linear function of time). The $\alpha_2(1-y)\frac{x^{n_2}}{K_2^{n_2}+x^{n_2}}$ term in Eq. [2] captures the activation of chemical y by chemical x. Note that this term contains a Hill function which is simply a sigmoidal function of x. As the level of chemical x goes from low levels to medium levels, the activation rate of y increases relatively quickly but as chemical x goes from medium levels to high levels, the activation rate of y increases more slowly and eventually reaches a maximum. The $-\beta_1 x\frac{y^{n_1}}{K_1^{n_1}+y^{n_1}}$ term in Eq. [1] models the deactivation of chemical x by chemical y which is the negative feedback portion of the system. Finally, the $-\beta_2 y$ term in Eq. [2] models the deactivation of chemical y.

$$\frac{dx}{dt} = \alpha_1 - \beta_1 x\frac{y^{n_1}}{K_1^{n_1}+y^{n_1}}, \qquad \textbf{[1]}$$

$$\frac{dy}{dt} = \alpha_2(1-y)\frac{x^{n_2}}{K_2^{n_2}+x^{n_2}} - \beta_2 y. \qquad \textbf{[2]}$$

The above model itself, however, did not produce sustained oscillations for many positive parameter values tested (Ferrell, Tsai and Yang, 2011). Only when a third chemical (three-ODE extension, bi-stable trigger) or an undefined time delay (2-DDE extension) is added to the system, can it produce sustained oscillations (Ferrell, Tsai and Yang, 2011). In the course of further investigating this model, we have found mathematically that this model indeed cannot produce sustained oscillations (App. A).

The role of short periodic reaction pauses in generating long oscillations

The failure of the above two-ODE to account for biological oscillations seems to be at odds with experimental evidence, such as the oscillations observed with the Hes1 and Hes7 auto negative feedback loops. We hypothesized that the reason for this failure is that a general characteristic of biochemical reactions, i.e., the discreteness of the reactions, is missing from the model. Discreteness is likely an important and yet overlooked feature of biochemical reactions as discussed earlier.

To modify the above model to accommodate the stop-start nature of biochemical reactions, we assume that one or more of the coefficients in Eqs. [1] and [2] are periodic with the period(s) in the range of a few seconds, and the system to be modeled is in a sufficiently small space inside the cell so that all the molecules of the same species act synchronously. Since the exact function of a periodic coefficient is unknown, we first test three common periodic functions for the α_1 coefficient in the two-ODE system, including a sine pulse, a triangle pulse, and a sawtooth pulse with a pausing period of 3 seconds (when $P(t) = 0$), App. B). In all three cases, a sustained oscillation with an approximately 1-hour period is generated (Fig. 1). Interestingly, if we do not allow pauses (when $P(t) > 0$ at all time), no sustained oscillation can be obtained for a wide range of parameters in the two-ODE system. Pausing in a periodic coefficient, therefore, is sufficient and likely required for the two-ODE system to generate sustained long oscillations.

For further investigating the role of short periodic coefficients in generating sustained long oscillations, as a proof of concept, we use a Fourier series to model $P(t)$. Even though we do not directly use the Fourier series representation of $P(t)$ in our subsequent numerical experiments, we develop it in recognition that the true form of the pulsate function is unknown and Fourier series are the most flexible and robust method for modeling periodic functions. Here we assume that $P(t)$ resembles a piece-wise constant function (App. B) that has a pulse phase with a constant positive value θ alternating with a pause phase with a constant value 0. The pulse phase has a time length t_f and the pause phase a time length t_d. One complete period of the pulsate function is $t_f + t_d$. Such a function should capture the essential discreteness of the proposed pulsate behavior and also allows us to apply the asymptotic theory of Fourier series to avoid long equations and thus save computational time. In order to find the Fourier coefficients of $P(t)$, we turn to the field of electronics where rectangular waves are called rectangular pulse trains. We appropriate the formula for pulse trains to obtain Eq. [3] (App. C)

$$P(t) \sim \theta\left[\frac{t_f}{t_d} + \sum_{k=1}^{K} \frac{2}{\pi k}\sin\left(\frac{\pi k t_f}{t_d}\right)\cos\left(\frac{2\pi k}{t_d}\left(t - \frac{t_f}{2}\right)\right)\right]. \qquad \textbf{[3]}$$

PeerJ PrePrints

PeerJ PrePrints | https://dx.doi.org/10.7287/peerj.preprints.1272v1 | CC-BY 4.0 Open Access | rec: 29 Jul 2015, publ: 29 Jul 2015

Since $P(t)$ is discontinuous and therefore subject to the Gibbs phenomenon, i.e., the Fourier series approximation overshoots or undershoots discontinuous functions at the points of discontinuity (Foster and Richards, 1991; App C). In most applications, the numerical noise introduced by the Gibbs phenomenon is inconsequential, but in a non-linear system, small changes in parameters can potentially have dramatic effects on the behavior of the system. In order to mitigate the Gibbs phenomenon, we apply the technique of σ-approximation, which multiplies the periodic terms in the Fourier series by a "smoothing" factor that mitigates the over/undershooting (Hamming, 1987; App C). Applying this technique, we reach the following equation for the pulsate function,

$$P(t) \sim \theta\left[\frac{t_f}{t_d} + \sum_{k=1}^{m-1} \frac{2m}{(\pi k)^2} \sin\frac{\pi k}{m} \sin\left(\frac{\pi k t_f}{t_d}\right) \cos\left(\frac{2\pi k}{t_d}\left(t - \frac{t_f}{2}\right)\right)\right]. \quad \textbf{[4]}$$

When applying Eq. [4] to the coefficients in Eqs. [1] and [2], however, computing the thousands of terms of the Fourier series required to obtain an accurate approximation of $P(t)$ is computationally taxing and suffers from numerical noise. Alternatively, we apply the asymptotic theory of Fourier series to directly evaluate $P(t)$ without summing sines and cosines. This theory states that the Fourier series will converge to θ or 0 at continuous points but will converge to $\frac{\theta}{2}$ at points of discontinuity. Thus, we can model $P(t)$ directly as

$$P(t) = \begin{cases} \theta & \text{if} \quad t \bmod t_d > t_d - t_f \\ \frac{\theta}{2} & \text{if} \quad t \bmod t_d = 0 \quad \text{or} \quad t \bmod t_d = t_d - t_f \\ 0 & \text{otherwise} \end{cases}. \quad \textbf{[5]}$$

We replace, in turn, each coefficient (α_1,α_2,β_1,β_2) in Eqs. [1] and [2] with Eq. [5] so that each two-ODE model would have a single pulsate term, and numerically integrated each model with arbitrary parameters and initial conditions $x = y = 0$ (Fig. 2). These and earlier numerical integration results together show that replacing any coefficient with a pulsate term that pulses on the scale of seconds can induce stable system-wide oscillations with period lengths of approximately one to several hours.

Combinations of pulsate coefficients also produce sustained long oscillations

We also numerically integrate Eqs. [1] and [2] with two pulsate terms by replacing each possible pair of coefficients with Eq. [5] (Fig. 3). Parameters can be found for generating stable oscillations for all the pulsate term combinations, although the combinations of α_2 and β_2 and β_1 and β_2 yield erratic oscillations (in Fig. 3D and F).

When pulsate α_1,α_2,and β_2 terms are introduced into the model, stable oscillations can be produced with a set of the parameter values (Fig. 4A). Pulsate α_1,α_2,and β_1 terms can also produce stable but weak oscillations for another set of the parameter values (Fig. 4B). Attempts to find stable oscillations with the other possible combinations of three or four pulsate terms were unsuccessful.

Our results show that one or more pulsate coefficients representing short reaction pauses in the two-component negative feedback loop can produce sustained oscillations with

PeerJ PrePrints

PeerJ PrePrints | https://dx.doi.org/10.7287/peerj.preprints.1272v1 | CC-BY 4.0 Open Access | rec: 29 Jul 2015, publ: 29 Jul 2015

approximately one to several hours long periods for both x and y. The failure to demonstrate the same system behavior with all the possible combinations of the pulsate coefficients suggests that either not all coefficients should be pulsate in the system (which can be reasonably argued to be the case in the cell) or we simply have not found the appropriate parameter values.

The effect of periodic coefficients has previously been analyzed in predator-prey models (Cushing, 1977), which shows that periodic coefficients can lead to an oscillatory behavior. However, it only shows that ω-periodic coefficients can lead to ω-periodic solutions. In other words, the individual coefficients and the solutions have the same period in the predator-prey models. Our model, on the other hand, shows that short-duration pulses in coefficients can lead to long-duration oscillations in the system.

Comparison between our two-ODE model and the two-DDE model

Why does the addition of short-duration pulsate behavior create long-duration oscillations in the otherwise stable system? We conjecture that this is due to the diffusion-based pulsate behavior acting as a time delay. It is known that the two-ODE system with constant coefficients is stable unless there is some form of time delay between the two legs of the system either through adding a buffer chemical, or an explicit time delay in the form of delay differential equations (DDE) (Ferrell, Tsai and Yang, 2011). To explore our conjecture, we demonstrate the similarities between a two-DDE system and the two-ODE system with the diffusion-based pulsate behavior. Fig. 5A and B show, respectively, the results of numerically integrating the following two-DDE system (Eqs. [6] and [7]) from (Ferrell, Tsai and Yang, 2011) with a short time and a long time lag and otherwise identical parameters.

$$\frac{dx[t]}{dt} = \alpha_1 - \beta_1 x[t] \frac{y[t-\tau_1]^{n_1}}{K_1^{n_1} + y[t-\tau_1]^{n_1}}, \qquad \textbf{[6]}$$

$$\frac{dy[t]}{dt} = \alpha_2 (1 - y[t]) \frac{x[t-\tau_2]^{n_2}}{K_2^{n_2} + x[t-\tau_2]^{n_2}} - \beta_2 y[t]. \qquad \textbf{[7]}$$

We also numerically integrated the two-ODE pulsate system (Eqs. [1] and [2]) with short and long periods of the pulsate function and otherwise identical parameters (Fig. 5C and D). It is apparent that increasing the time lag in the two-DDE system has the same qualitative effect as increasing the period of the pulsate behavior in the two-ODE system: increasing the oscillation period and the peak height. However, peaks produced by our model are not as uniform as those produced by the two-DDE model in height and temporal separation. Also, in the limit of the two-DDE system where $\tau \rightarrow 0$, the system approaches the two-ODE system without pulsate behavior which is known to be stable. Correspondingly, as $t_f \rightarrow t_d$ in the two-ODE pulsate system it also approaches the stable two-ODE system. Even though both the two-DDE and our two-ODE models can produce similar oscillation outcomes, our two-ODE model is based clearly on a physical mechanism whereas the two-DDE model is not. It is envisioned that in more complex systems with numerous chemicals and multiple feedback loops, integration of additional $P(t)$ terms into expanded ODE models can be readily justified, which is not the case with the time delay factors, τs, in expanded DDE models.

Expansion of our model to a three-ODE system

To investigate how increasing complexity affects our model, we expanded the two-ODE model to a three-ODE model by modifying another model proposed by Ferrell, Tsai and Yang (2011), the three-ODE model with a buffer chemical. The third chemical in the system, z, acts as a buffer between x and y, and provides the necessary time delay which allows the system to oscillate. The three-ODE system from Ferrell, Tsai and Yang (2011) is

$$\frac{dx}{dt} = \alpha_1 - \beta_1 x \frac{y^{n_1}}{K_1^{n_1} + y^{n_1}}, \qquad \textbf{[8]}$$

$$\frac{dy}{dt} = \alpha_2 (1-y) \frac{z^{n_2}}{K_2^{n_2} + z^{n_2}} - \beta_2 y, \qquad \textbf{[9]}$$

$$\frac{dz}{dt} = \alpha_3 (1-z) \frac{x^{n_3}}{K_3^{n_3} + x^{n_3}} - \beta_3 z. \qquad \textbf{[10]}$$

In one form of our model, α_1, α_2, and α_3 are replaced with $P_1(t)$, $P_2(t)$, and $P_3(t)$ respectively, which gives us the system

$$\frac{dx}{dt} = P_1(t) - \beta_1 x \frac{y^{n_1}}{K_1^{n_1} + y^{n_1}}, \qquad \textbf{[11]}$$

$$\frac{dz}{dt} = P_2(t)(1-z) \frac{x^{n_2}}{K_2^{n_2} + x^{n_2}} - \beta_2 z, \qquad \textbf{[12]}$$

$$\frac{dy}{dt} = P_3(t)(1-y) \frac{z^{n_3}}{K_3^{n_3} + z^{n_3}} - \beta_3 y. \qquad \textbf{[13]}$$

We numerically integrate both Ferrell et al.'s model (Eqs. [8-10]; Fig. 6A) and our model (Eqs. [11-13]; Fig. 6B). All parameters are identical and the pulsate terms in Eqs. [11-13] are calibrated so that their average values are equal to the respective α_1 α_2, and α_3 in Eqs. [8-10]. The results show that adding pulsate behavior to models that already oscillate increases the peak height and period of the oscillation comparing to what they would have been without the pulsate behavior. As another comparison, we also numerically integrate the following analogous three-DDE model (Eqs. [14-16]; Fig. 6C) and our three-ODE model (Fig. 6D) with a different but identical set of parameters, except that the former does not involve pulsate terms and the latter involves pulsate α_1 α_2, and α_3. The peak height and period of the oscillation from the three-DDE model are still shorter than those from our three-ODE model, even though they are longer than those from the vanilla three-ODE model, respectively. These results provide further evidence that the molecular pulsate behavior can be an important physical basis for the time delay – and hence the oscillations – in many biological systems containing negative feedback loops.

$$\frac{dx[t]}{dt} = \alpha_1 - \beta_1 x[t] \frac{y[t-\tau_1]^{n_1}}{K_1^{n_1} + y[t-\tau_1]^{n_1}}, \qquad \textbf{[14]}$$

PeerJ PrePrints

PeerJ PrePrints | https://dx.doi.org/10.7287/peerj.preprints.1272v1 | CC-BY 4.0 Open Access | rec: 29 Jul 2015, publ: 29 Jul 2015

$$\frac{dz[t]}{dt} = \alpha_2(1 - z[t])\frac{x[t-\tau_2]^{n_2}}{K_2^{n_2} + x[t-\tau_2]^{n_2}} - \beta_2 z[t] \; , \qquad \textbf{[15]}$$

$$\frac{dy[t]}{dt} = \alpha_3(1 - y[t])\frac{z[t-\tau_3]^{n_3}}{K_3^{n_3} + z[t-\tau_3]^{n_3}} - \beta_3 y[t]. \qquad \textbf{[16]}$$

CONCLUSIONS

Our ODE model indicates that a negative feedback loop and short (a few seconds) reaction pauses are sufficient for generating sustained long (hours) oscillations that resemble actual oscillations in biological systems.

REFERENCES

Albeck JG, Mills GB, Brugge JS. (2013) Frequency-modulated pulses of ERK activity transmit quantitative proliferation signals. *Mol Cell* 49:249-261.

Bessho Y, Hirata H, Masamizu Y, Kageyama R. (2003) Periodic repression by the bHLH factor Hes7 is an essential mechanism for the somite segmentation clock. *Genes Dev* 17:1451-1456.

Cushing JM. (1977) Periodic time-dependent predator-prey systems. *SIAM J Appl Math* 32:82-95.

Engler D, Pham T, Fullerton MJ, Clarke IJ, Funder JW. (1989) Evidence for an ultradian secretion of adrenocorticotropin, beta-endorphin and alpha-melanocyte-stimulating hormone by the ovine anterior and intermediate pituitary. *Neuroendocrinology* 49:349–360.

Ferrell JE Jr, Tsai TY, Yang Q. (2011) Modeling the cell cycle: why do certain circuits oscillate? *Cell* 144:874-885.

Foster J, Richards FB. (1991) The Gibbs Phenomenon for piecewise-linear approximation. *Amer Math Monthly* 98:47-49.

Hamming RW. (1987) *Numerical Methods for Scientists and Engineers, 2nd edition,* Dover, New York, pp. 534-536.

Harima Y, Takashima Y, Ueda Y, Ohtsuka T, Kageyama R. (2013) Accelerating the tempo of the segmentation clock by reducing the number of introns in the Hes7 gene. *Cell Rep* 3:1-7.

Harima Y, Imayoshi I, Shimojo H, Kobayashi T, Kageyama R. (2014) The roles and mechanism of ultradian oscillatory expression of the mouse Hes genes. *Semin Cell Dev Biol* 34:85-90.

Jasper MS, Engeland WC. (1991) Synchronous ultradian rhythms in adrenocortical secretion detected by microdialysis in awake rats. *Am J Physiol* 261:R1257–R1268.

Kerssemakers JW, Munteanu EL, Laan L, Noetzel TL, Janson ME, Dogterom M. (2006) Assembly dynamics of microtubules at molecular resolution. *Nature* 442:709–712.

Kou SC, Xie XS. (2004) Generalized Langevin equation with fractional Gaussian noise: subdiffusion within a single protein molecule. *Phys Rev Lett* 93:180603.

Neuman KC, Abbondanzieri EA, Landick R, Gelles J, Block SM. (2003) Ubiquitous transcriptional pausing is independent of RNA polymerase backtracking. *Cell* 115:437-47.

Schek III HT, Gardner MK, Cheng J, Odde DJ, Hunt AJ. (2007) Microtubule assembly dynamics at the nanoscale. *Curr Biol* 17:1445–1455.

PeerJ PrePrints

Takashima Y, Ohtsuka T, González A, Miyachi H, Kageyama R. (2011) Intronic delay is essential for oscillatory expression in the segmentation clock. *Proc Natl Acad Sci U S A* 108:3300-3305.
Tapp WN, Holaday JW, Natelson BH. (1984) Ultradian glucocorticoid rhythms in monkeys and rats continue during stress. *Am J Physiol Regul Integr Comp Physiol* 247:R866–R871.
Weitzman ED, Fukushima D, Nogeire C, Roffwarg H, Gallagher TF, Hellman L. (1971) Twenty-four hour pattern of the episodic secretion of cortisol in normal subjects. *J Clin Endocrinol Metab* 33:14–22.
Yang H, Luo G, Karnchanaphanurach P, Louie TM, Rech I, Cova S, Xun L, Xie XS. (2003) Protein conformational dynamics probed by single-molecule electron transfer. *Science* 302:262–266.
Yang M. (2014) Slow diffusion underlies alternation of fast and slow growth periods of microtubule assembly. *ScientificWorldJournal* doi: 10.1155/2014/601898.

PeerJ PrePrints

PeerJ PrePrints

APPENDICES

Appendix A: Proof that the two-ODE System with constant coefficients cannot generate stable limit cycles

We can use linear stability analysis to show that the two-ODE system with constant coefficients cannot generate stable limit cycles. According to linear stability analysis, the stability of the two-ODE system can be deduced from the Jacobian matrix of the system.

Assume that $\alpha_1, \alpha_2, \beta_1, \beta_2 > 0$; $n_1, n_2 > 2$; and $x, y \geq 0$. Let (x, y) be a critical point of the two-ODE system. First, we compute the Jacobian by computing all of the partial derivatives. Put

$$f(x,y) = \frac{\delta x}{\delta t} = \alpha_1 - \beta_1 x \frac{y^{n_1}}{K_1^{n_1} + y^{n_1}},$$

$$g(x,y) = \frac{\delta y}{\delta t} = \alpha_2 (1 - y) \frac{x^{n_2}}{K_2^{n_2} + x^{n_2}} - \beta_1 y.$$

Then, we compute each partial derivative:

$$\frac{\delta f}{\delta x} = -\beta_1 \frac{y^{n_1}}{K_1^{n_1} + y^{n_1}},$$

$$\frac{\delta f}{\delta y} = \beta_1 x \frac{K_1^{n_1} n_1 y^{n_1 - 1}}{\left(K_1^{n_1} + y^{n_1}\right)^2},$$

$$\frac{\delta g}{\delta x} = a_2 (1 - y) \frac{K_2^{n_2} n_2 x^{n_2 - 1}}{\left(K_2^{n_2} + x^{n_2}\right)^2},$$

$$\frac{\delta g}{\delta y} = -\alpha_2 \frac{x^{n_2}}{K_2^{n_2} + x^{n_2}} - \beta_2.$$

Then, the Jacobian, J is

PeerJ PrePrints | https://dx.doi.org/10.7287/peerj.preprints.1272v1 | CC-BY 4.0 Open Access | rec: 29 Jul 2015, publ: 29 Jul 2015

PeerJ PrePrints

$$J = \begin{bmatrix} -\beta_1 \dfrac{y^{n_1}}{K_1^{n_1} + y^{n_1}} & \beta_1 x \dfrac{K_1^{n_1} n_1 y^{n_1 - 1}}{\left(K_1^{n_1} + y^{n_1}\right)^2} \\ \alpha_2 (1 - y) \dfrac{K_2^{n_2} n_2 x^{n_2 - 1}}{\left(K_2^{n_2} + x^{n_2}\right)^2} & -\alpha_2 \dfrac{x^{n_2}}{K_2^{n_2} + x^{n_2}} - \beta_2 \end{bmatrix}$$

and the eigenvalues of the matrix are

$$\lambda_{1,2} = \frac{\mathrm{tr}\,(J)}{2} \pm \sqrt{\frac{\mathrm{tr}\,(J)^2}{4} - \det(J)}.$$

In order to generate sustained oscillations at least one eigenvalue must have non-negative real part and non-zero imaginary part. So there must be some i such that, $\mathrm{Re}\,(\lambda_i) \geq 0$ and $\mathrm{Im}\,(\lambda_i) \neq 0$. First, we show that $\mathrm{tr}\,(J) < 0$.

$$\mathrm{tr}\,(J) = -\beta_1 \frac{y^{n_1}}{K_1^{n_1} + y^{n_1}} - \alpha_2 \frac{x^{n_2}}{K_2^{n_2} + x^{n_2}} - \beta_2.$$

Since all parameters are positive, each of the terms are negative and thus $\frac{\mathrm{tr}\,(J)}{2} < 0$.

Now, let $R = \frac{\mathrm{tr}\,(J)^2}{4} - \det(J)$. Suppose that $R < 0$, then $\sqrt{R}$ is imaginary so that $\mathrm{Re}\,(\lambda_i) = \frac{\mathrm{tr}\,(J)}{2} < 0$ for each i. Suppose that $R \geq 0$, then $\sqrt{R}$ is real and $\mathrm{Re}\,(\lambda_i) = \frac{\mathrm{tr}\,(J)}{2} \pm \sqrt{R}$ while $\mathrm{Im}\,(\lambda_i) = 0$. We see that none of the cases satisfies the conditions for sustained oscillations. Thus, the two-ODE system cannot generate sustained oscillations.

Appendix B: Pulsate functions used for coefficients in the two-ODE and related systems

Sine pulse

$$P(t) = \begin{cases} \theta \left| \sin\left(\dfrac{\pi t}{t_f}\right) \right| & \text{if } t \bmod (t_f + t_d) \leq t_f \\ 0 & \text{otherwise} \end{cases}.$$

PeerJ PrePrints | https://dx.doi.org/10.7287/peerj.preprints.1272v1 | CC-BY 4.0 Open Access | rec: 29 Jul 2015, publ: 29 Jul 2015

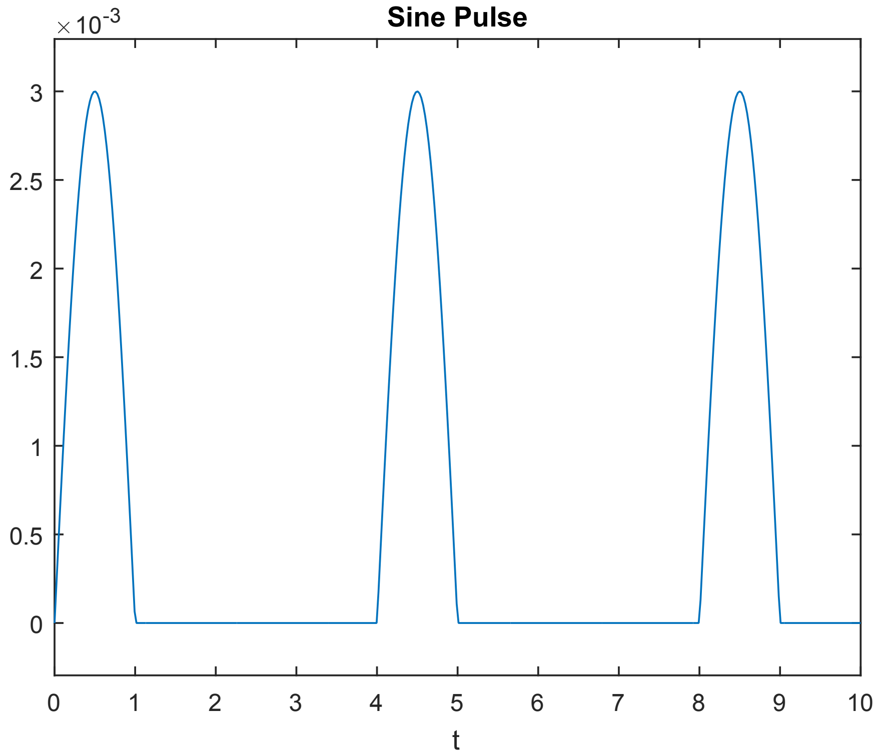

Triangle pulse

$$P(t) = \begin{cases} \frac{2\theta}{t_f}\left(t \bmod \frac{t_f}{2}\right) & \text{if} \quad t \bmod (t_f + t_d) \leq \frac{t_f}{2} \\ \frac{-2\theta}{t_f}\left(t \bmod \frac{t_f}{2}\right) + \theta & \text{if} \quad t_f \geq t \bmod (t_f + t_d) > \frac{t_f}{2}. \\ 0 \text{ otherwise} \end{cases}$$

PeerJ PrePrints

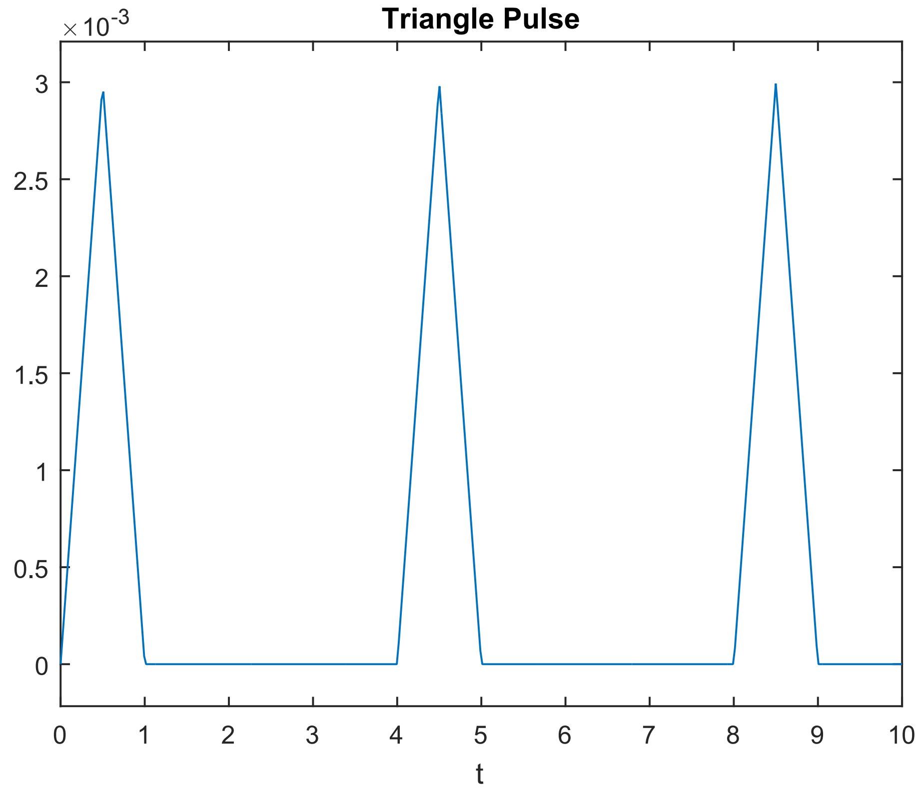

Sawtooth pulse

$$P(t) = \begin{cases} \frac{\theta}{t_f}(t \bmod t_f) & \text{if } t \bmod (t_f + t_d) \leq t_f \\ 0 & \text{otherwise} \end{cases}.$$

PeerJ PrePrints | https://dx.doi.org/10.7287/peerj.preprints.1272v1 | CC-BY 4.0 Open Access | rec: 29 Jul 2015, publ: 29 Jul 2015

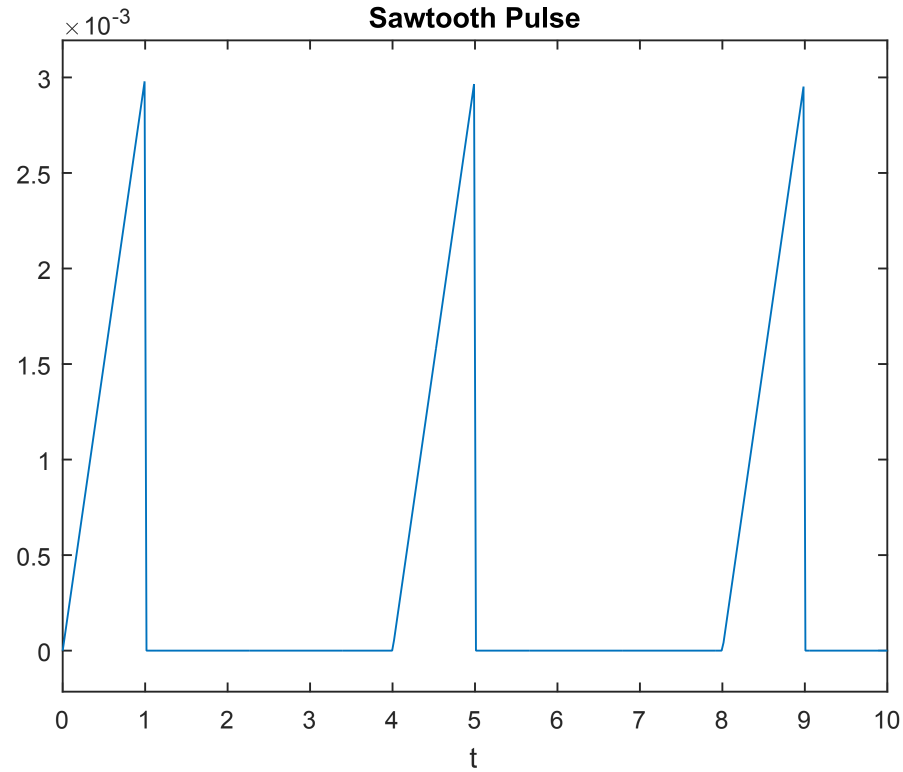

Piece-wise pulse

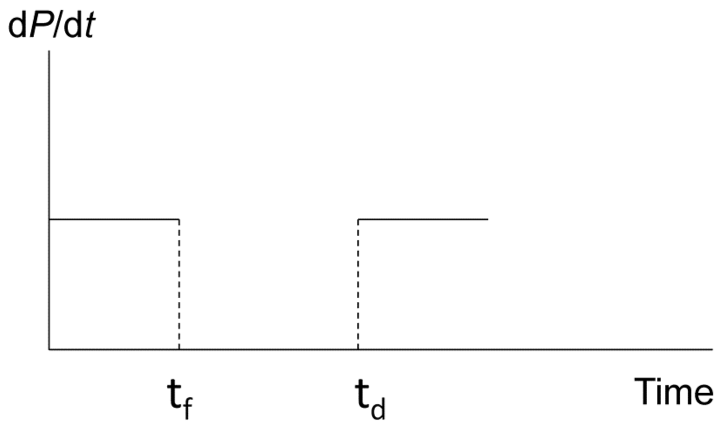

Appendix C: Derivation of the Pulsate Function: Pulse Trains, Gibbs Phenomenon, and σ-Approximation

Pulse trains

The pulsate function, $P(t)$, can be represented by the general Fourier series

$$\frac{dP}{dt} \sim A_0 + \sum_{k=1}^{\infty} A_k \cos\left(\frac{2\pi kt}{t_d}\right) + B_k \sin\left(\frac{2\pi kt}{t_d}\right). \qquad [A.1]$$

PeerJ PrePrints

Where the coefficients can be calculated with the formulas

$$A_0 = \frac{1}{2t_d}\int_{-t_d}^{t_d} \frac{dP}{dt}dt, \quad \text{[A.2]}$$

$$A_k = \frac{1}{t_d}\int_{-t_d}^{t_d} \frac{dP}{dt}\cos\left(\frac{2\pi kt}{t_d}\right)dt, \quad \text{[A.3]}$$

$$B_k = \frac{1}{t_d}\int_{-t_d}^{t_d} \frac{dP}{dt}\sin\left(\frac{2\pi kt}{t_d}\right)dt. \quad \text{[A.4]}$$

The ~ symbol means that the Fourier series will converge to the target function in the limit, except at discontinuities where it will converge to the average of the two discontinuous points. We used these formulas to calculate the coefficients for a rectangular wave. We first calculated the coefficients for a simple wave that has amplitude [0, 1] and is symmetric about the P-axis (so it starts halfway through the first pulse at $t = 0$) and then we shifted and scaled the Fourier series accordingly.

Calculating A_0:

$$A_0 = \frac{1}{2t_d}\int_{-t_d}^{t_d} P(t)dt$$

$$= \frac{1}{2t_d}\int_{-t_f}^{t_f} 1dt$$

$$= \frac{t_f}{t_d}.$$

Calculating A_k:

$$A_k = \frac{1}{t_d}\int_{-t_d}^{t_d} P(t)\cos\left(\frac{2\pi kt}{t_d}\right)dt$$

$$= \frac{1}{t_d}\left[\int_{-t_f/2}^{t_f/2} \cos\left(\frac{2\pi kt}{t_d}\right)dt + \int_{t_d - t_f/2}^{t_d} \cos\left(\frac{2\pi kt}{t_d}\right)dt + \int_{-t_d}^{-t_d + t_f/2} \cos\left(\frac{2\pi kt}{t_d}\right)dt\right]$$

$$= \frac{2}{t_d}\int_{-t_f/2}^{t_f/2} \cos\left(\frac{2\pi kt}{t_d}\right)dt$$

$$= \frac{2}{t_d}\frac{t_d}{2\pi k}\left[\sin\left(\frac{\pi kt_f}{t_d}\right) + \sin\left(\frac{\pi kt_f}{t_d}\right)\right]$$

$$= \frac{2}{k\pi}\sin\left(\frac{\pi kt_f}{t_d}\right).$$

PeerJ PrePrints | https://dx.doi.org/10.7287/peerj.preprints.1272v1 | CC-BY 4.0 Open Access | rec: 29 Jul 2015, publ: 29 Jul 2015

Calculating B_k: The term $B_k \sin \frac{2\pi kt}{t_d}$ is the odd part of $P(t)$. However, we have defined $P(t)$ to be symmetric about the P-axis and therefore entirely even. Since the function has no odd part, we know that $B_k = 0$.

Finally, we scale the Fourier series by β so that its amplitude is $[0, \beta]$ and we shift it by $t_f/2$ so that it starts with one complete pulse. This gives us the formula

$$P(t) \sim \beta\left[\frac{t_f}{t_d} + \sum_{k=1}^{\infty} \frac{2}{k\pi} \sin\left(\frac{\pi k t_f}{t_d}\right) \cos\left(\frac{2\pi k}{T}\left(t - \frac{t_f}{2}\right)\right)\right]. \quad \text{[A.5]}$$

Mitigating the Gibbs phenomenon

The pulsate function Fourier series suffers from the Gibbs phenomenon, which is the overshooting/undershooting of the Fourier series at points of discontinuity (Foster and Richards, 1991). In order to mitigate this, we applied the technique of σ-approximation which multiplies the periodic portions of the Fourier series by a smoothing factor – the Lanczos σ factor (Hamming, 1987) – which is defined as

$$\sigma = \operatorname{sinc}\left(\frac{k}{m}\right) = \frac{\sin \frac{k\pi}{m}}{\frac{k\pi}{m}} = \frac{m \sin \frac{k\pi}{m}}{k\pi}. \quad \text{[A.6]}$$

Here m is the order of the finite-order Fourier series plus one. Now, we reach the final form

$$\frac{dP}{dt} \sim \beta\left[\frac{t_f}{t_d} + \sum_{k=1}^{m-1} \sigma \frac{2}{k\pi} \sin\left(\frac{\pi k t_f}{t_d}\right) \cos\left(\frac{2\pi k}{T}\left(t - \frac{t_f}{2}\right)\right)\right] \quad \text{[A.7]}$$

$$= \beta\left[\frac{t_f}{t_d} + \sum_{k=1}^{m-1} \frac{2m}{(\pi k)^2} \sin\left(\frac{\pi k}{m}\right) \sin\left(\frac{\pi k t_f}{t_d}\right) \cos\left(\frac{2\pi k}{T}\left(t - \frac{t_f}{2}\right)\right)\right].$$

For an illustration of the difference between the σ-approximated Fourier series and the unadjusted Fourier series see Fig. A.1, which shows a zoomed-in plot of $P(t)$ during one of its pulses. The σ-approximated series is a perfect horizontal line, while the unadjusted series has some unwanted curvature. For an illustration of the numerical noises' impact on the integration, see Fig. A.2, which shows two versions of a two-ODE pulsate model with the exact same parameters except one model's Fourier series are σ-approximated while the other model's Fourier series are not. The seemingly insignificant numerical noise introduced by the Gibbs phenomenon has a large effect on the final results, so it must be reduced.

PeerJ PrePrints

PeerJ PrePrints

A

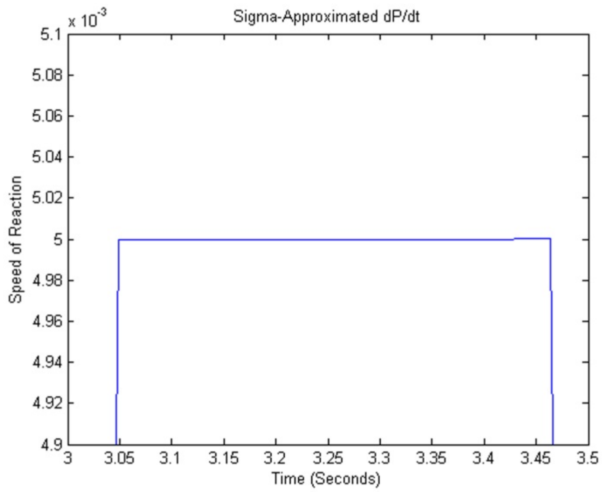

B

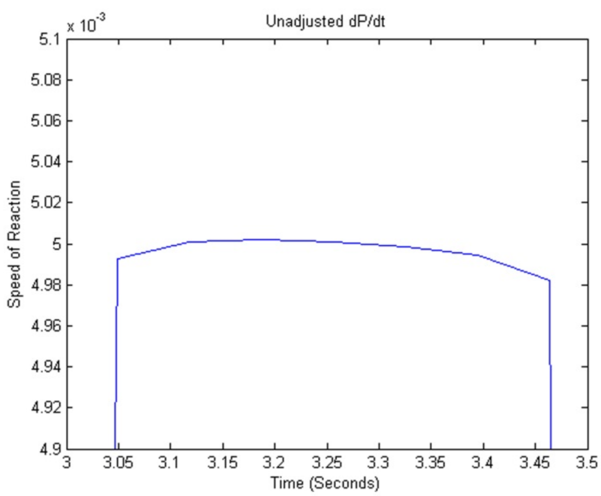

Fig. A.1. Comparison between dP/dt with and without σ-approximation. (A) Zoomed-in plot of σ-approximated dP/dt with $t_f = 0.5$, $t_d = 3$, $\beta = 0.005$, and $m = 1000$. (B) Zoomed-in plot of unadjusted dP/dt with the same parameters as A.

A

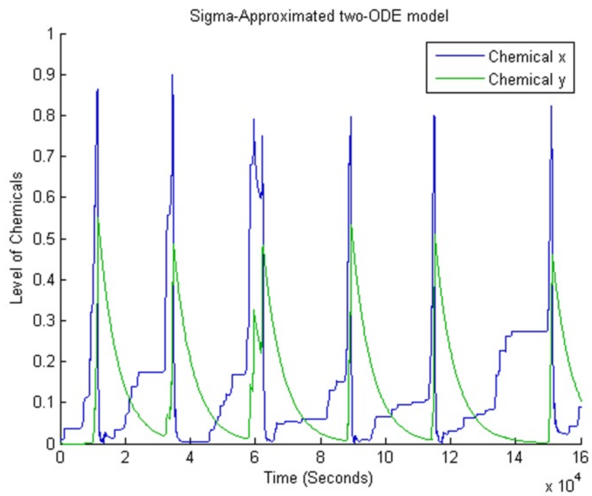

B

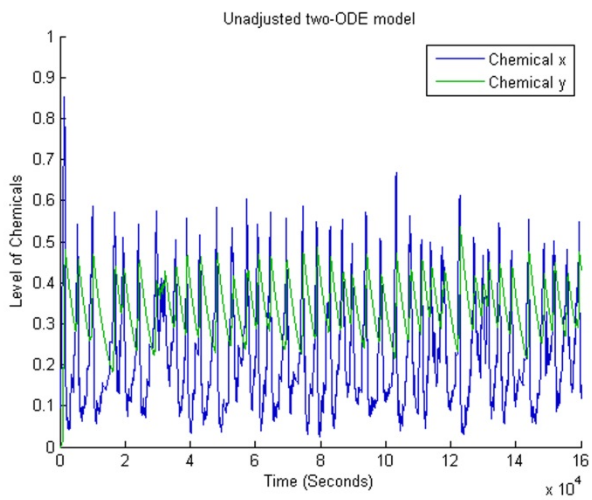

Fig. A.2. Comparison between models with and without σ-approximation. (A) Numerical integration of equations [5] and [6] with σ-approximated pulsate terms and arbitrarily chosen parameters $t_{f1} = 0.5$, $t_{d1} = 3$, $\theta_1 = 0.005$, $\beta_1 = 0.0125$, $K_1 = 0.5$, $n_1 = 8$, $m_1 = 1000$ for [5] and $t_{f2} = 0.5$, $t_{d2} = 4$, $\theta_2 = 0.02$, $\beta_2 = 0.0001666667$, $K_2 = 0.5$, $n_2 = 8$, $m_2 = 1000$ for [6]. (B) Same as (A) except the pulsate terms are not σ-approximated.

PeerJ PrePrints

Figure legends

Figure 1. Numerical integration of Eqs. [1] and [2] with α_1 being replaced by a pulsate function. (A) α_1 is a sine pulse. Initial $x = t = 0$, and $y = 0.3$. The parameter values are $t_{f1} = 1$, $t_{d1} = 1$, $\theta_1 = 0.002$, $\beta_1 = 0.025$, $K_1 = 0.5$, $n_1 = 8$ for Eq. [1] and $\alpha_2 = 0.0001$, $\beta_2 = 0.0001$, $K_2 = 0.5$, $n_2 = 8$ for Eq. [2]. (B) α_1 is a triangle pulse. Initial $x = t = 0$, and $y = 0.35$. The parameter values are $t_{f1} = 1$, $t_{d1} = 1$, $\theta_1 = 0.0025$, $\beta_1 = 0.025$, $K_1 = 0.5$, $n_1 = 8$ for Eq. [1] and $\alpha_2 = 0.0001$, $\beta_2 = 0.0001$, $K_2 = 0.5$, $n_2 = 8$ for Eq. [2]. (C) α_1 is a sawtooth pulse. Initial $x = t = 0$, and $y = 0.25$. The parameter values are $t_{f1} = 1$, $t_{d1} = 1$, $\theta_1 = 0.003$, $\beta_1 = 0.025$, $K_1 = 0.5$, $n_1 = 8$ for Eq. [1] and $\alpha_2 = 0.0002$, $\beta_2 = 0.0001$, $K_2 = 0.5$, $n_2 = 8$ for Eq. [2].

Figure 2. Numerical integration of Eqs. [1] and [2] with single constant coefficients replaced by pulsate terms. (A) α_1 is replaced by the pulsate function $P_1(t)$. The parameter values are $t_{f1} = 0.25$, $t_{d1} = 1$, $\theta_1 = 0.003$, $\beta_1 = 0.015$, $K_1 = 0.5$, $n_1 = 8$ for Eq. [1] and $\alpha_2 = 0.003$, $\beta_2 = 0.0001$, $K_2 = 0.5$, $n_2 = 8$ for Eq. [2]. (B) α_2 is replaced by the pulsate function $P_2(t)$. The parameter values are $\alpha_1 = 0.0001$, $\beta_1 = 0.05$, $K_1 = 0.5$, $n_1 = 8$ for Eq. [1] and $t_{f2} = 0.25$, $t_{d2} = 1$, $\theta_2 = 0.01$, $\beta_2 = 0.0001$, $K_2 = 0.5$, $n_2 = 8$ for Eq. [2]. (C) β_1 is replaced by the pulsate function $P_1(t)$. The parameter values are $\alpha_1 = 0.0001$, $t_{f1} = 0.25$, $t_{d1} = 1$, $\theta_1 = 0.4$, $K_1 = 0.5$, $n_1 = 8$ for Eq. [1] and $\alpha_2 = 0.011$, $\beta_2 = 0.0002$, $K_2 = 0.5$, $n_2 = 8$ for Eq. [2]. (D) β_2 is replaced by the pulsate function $P_2(t)$. The parameter values are $\alpha_1 = 0.0001$, $\beta_1 = 0.01$, $K_1 = 0.5$, $n_1 = 8$ for Eq. [1] and $\alpha_2 = 0.0007$, $t_{f2} = 0.25$, $t_{d2} = 1$, $\theta_2 = 0.01$, $K_2 = 0.5$, $n_2 = 8$ for Eq. [2]. The initial conditions are always $x = y = t = 0$.

Figure 3. Numerical integration of Eqs. [1] and [2] with pairs of constant coefficients replaced by pulsate terms. (A) α_1 and β_1 are replaced by the pulsate functions $P_{11}(t)$ and $P_{12}(t)$, respectively. The parameter values are $t_{f11} = 0.25$, $t_{d11} = 1$, $\theta_{11} = 0.001$, $t_{f12} = 0.25$, $t_{d12} = 1.25$, $\theta_{12} = 0.05$, $K_1 = 0.5$, $n_1 = 8$ for Eq. [1] and $\alpha_2 = 0.0003$, $\beta_2 = 0.0002$, $K_2 = 0.5$, $n_2 = 8$ for Eq. [2]. (B) α_1 and β_2 are replaced by the pulsate functions $P_{11}(t)$ and $P_{22}(t)$, respectively. The parameter values are $t_{f11} = 0.5$, $t_{d11} = 3$, $\theta_{11} = 0.0025$, $\beta_1 = 0.001$, $K_1 = 0.5$, $n_1 = 8$ for Eq. [1] and $\alpha_2 = 0.001$, $t_{f22} = 0.5$, $t_{d22} = 4$, $\theta_{22} = 0.005$, $K_2 = 0.5$, $n_2 = 8$ for Eq. [2]. (C) β_1 and α_2 are replaced by the pulsate functions $P_{12}(t)$ and $P_{21}(t)$, respectively. The parameter values are $\alpha_1 = 0.00005$, $t_{f12} = 0.5$, $t_{d12} = 3$, $\theta_{12} = 0.2$, $K_1 = 0.5$, $n_1 = 8$ for Eq. [1] and $t_{f21} = 0.5$, $t_{d21} = 4$, $\theta_{21} = 1$, $\beta_2 = 0.001$, $K_2 = 0.5$, $n_2 = 8$ for Eq. [2]. (D) α_2 and β_2 are replaced by the pulsate functions $P_{21}(t)$ and $P_{22}(t)$, respectively. The parameter values are $\alpha_1 = 0.0009$, $\beta_1 = 0.0133$, $K_1 = 0.5$, $n_1 = 8$ for Eq. [1] and $t_{f21} = 0.5$, $t_{d21} = 3$, $\theta_{21} = 0.3$, $t_{f22} = 0.5$, $t_{d22} = 4$, $\theta_{22} = 0.02$, $K_2 = 0.5$, $n_2 = 8$ for Eq. [2]. (E) α_1 and α_2 are replaced by the pulsate functions $P_{11}(t)$ and $P_{21}(t)$, respectively. The parameter values are $t_{f11} = 0.25$, $t_{d11} = 1$, $\theta_{11} = 0.0003$, $\beta_1 = 0.0125$, $K_1 = 0.5$, $n_1 = 8$ for Eq. [1] and $t_{f21} = 0.25$, $t_{d21} = 1.25$, $\theta_{21} = 0.00125$, $\beta_2 = 0.000014$, $K_2 = 0.5$, $n_2 = 8$ for Eq. [2]. (F) β_1 and β_2 are replaced by the pulsate functions $P_{12}(t)$ and $P_{22}(t)$, respectively. The parameter

PeerJ PrePrints | https://dx.doi.org/10.7287/peerj.preprints.1272v1 | CC-BY 4.0 Open Access | rec: 29 Jul 2015, publ: 29 Jul 2015

values are $\alpha_1 = 0.00007$, $t_{f12} = 0.25$, $t_{d12} = 1$, $\theta_{12} = 0.03$, $K_1 = 0.5$, $n_1 = 8$ for Eq. [1] and $\alpha_2 = 0.00025$, $t_{f22} = 0.25$, $t_{d22} = 1.25$, $\theta_{22} = 0.00015$, $K_2 = 0.5$, $n_2 = 8$ for Eq. [2]. The initial conditions are always $x = y = t = 0$.

Figure 4. Numerical integration of equations [1] and [2] with triples of constant coefficients replaced by pulsate terms. (A) α_1, α_2, and β_2 are replaced by the pulsate functions $P_{11}(t)$, $P_{21}(t)$, and $P_{22}(t)$, respectively. The parameter values are $t_{f11} = 0.5$, $t_{d11} = 3$, $\theta_{11} = 0.005$, $\beta_1 = 0.05$, $K_1 = 0.5$, $n_1 = 8$ for Eq. [1] and $t_{f21} = 0.5$, $t_{d21} = 4$, $\theta_{21} = 0.03$, $t_{f22} = 0.5$, $t_{d22} = 4.5$, $\theta_{22} = 0.001$, $K_2 = 0.5$, $n_2 = 8$ for Eq. [2]. (B) α_1, β_1, and α_2 are replaced by the pulsate functions $P_{11}(t)$, $P_{12}(t)$, and $P_{21}(t)$, respectively. The parameter values are $t_{f11} = 0.25$, $t_{d11} = 1$, $\theta_{11} = 0.00005$, , $t_{f12} = 0.25$, $t_{d12} = 1.5$, $\theta_{12} = 0.075$, $K_1 = 0.5$, $n_1 = 8$ for Eq. [1] and $t_{f21} = 0.25$, $t_{d21} = 1.25$, $\theta_{21} = 0.001$, $\beta_2 = 0.0002$, $K_2 = 0.5$, $n_2 = 8$ for Eq. [2]. The initial conditions are always $x = y = t = 0$.

Figure 5. A comparison between two-DDE models with varying time lags and two-ODE models with varying pulsate periods. Only chemical x has been plotted. Chemical y oscillates with the same period as x so it is excluded for clarity. (A) Numerical integration of DDE Eqs. [6] and [7] with arbitrarily chosen parameters $\tau_1 = 250$, $\alpha_1 = 0.0005$, $\beta_1 = 0.0125$, $K_1 = 0.5$, $n_1 = 8$ for Eq. [6] and $\tau_1 = 250$, $\alpha_2 = 3$, $\beta_2 = 0.02$, $K_2 = 0.5$, $n_2 = 8$ for Eq. [7]. (B) Numerical integration of DDE Eqs. [6] and [7] with the same parameters as in (A) except $\tau_1 = \tau_2 = 500$. (C) Numerical integration of ODE Eqs. [1] and [2] where α_1 and α_2 are replaced by the pulsate functions $P_{11}(t)$ and $P_{21}(t)$, respectively. The parameter values are $t_{f11} = 0.5$, $t_{d11} = 2.5$, $\theta_{11} = 0.005$, $\beta_1 = 0.0125$, $K_1 = 0.5$, $n_1 = 8$ for Eq. [1] and $t_{f21} = 0.5$, $t_{d21} = 2$, $\theta_{21} = 0.0175$, $\beta_2 = 0.0001666667$, $K_2 = 0.5$, $n_2 = 8$ for Eq. [2]. (D) Numerical integration of Eqs. [1] and [2] where α_1 and α_2 are replaced by the pulsate functions $P_{11}(t)$ and $P_{21}(t)$, respectively. The parameter values are $t_{f1} = 0.5$, $t_{d1} = 3$, $\theta_1 = 0.006$ for Eq. [1] and $t_{f2} = 0.5$, $t_{d2} = 3.5$, $\theta_2 = 0.0306$ for Eq. [2]. All other parameters are the same as in (C). The initial conditions are always $x = y = t = 0$. The parameter $\theta_i^{long} = \theta_i^{short} * t_d^{long} / t_d^{short}$ so that the average values of $P_i(t)$ in the long-period ODE pulsate model and the short-period ODE pulsate model are equal.

Figure 6. A comparison between three-ODE models, three-DDE models, and three-ODE models with varying pulsate periods. (A) Numerical integration of the standard three-ODE model, Eqs. [8-10], with arbitrarily chosen parameters $\alpha_1 = 0.0004166666667$, $\beta_1 = 0.0125$, $K_1 = 0.5$, $n_1 = 8$ for Eq. [8]; $\alpha_2 = 0.0025$, $\beta_2 = 0.0001666667$, $K_2 = 0.5$, $n_2 = 8$ for Eq. [9]; and $\alpha_3 = 0.003$, $\beta_3 = 0.0001666667$, $K_3 = 0.5$, $n_3 = 8$ for Eq. [10]. (B) Numerical integration of the three-ODE model, Eqs. [11-13], with arbitrarily chosen parameters $t_{f1} = 0.25$, $t_{d1} = 1$, $\theta_1 = 0.0017$ for Eq. [11]; $t_{f2} = 0.25$, $t_{d2} = 1.25$, $\theta_2 = 0.0125$ for Eq. [12]; and $t_{f3} = 0.25$, $t_{d3} = 1.5$, $\theta_3 = 0.018$ for Eq. [13] and with all other parameters unchanged from (A). (C) Numerical integration of the three-DDE model, Eqs. [14-16]. All parameters are the same as in (A) except $\tau_1 = \tau_2 = \tau_3 = 300$. (D) Numerical integration of the three-ODE model, Eqs. [11-13]

PeerJ PrePrints | https://dx.doi.org/10.7287/peerj.preprints.1272v1 | CC-BY 4.0 Open Access | rec: 29 Jul 2015, publ: 29 Jul 2015

with arbitrarily chosen parameters $t_{f1} = 0.5$, $t_{d1} = 3$, $\theta_1 = 0.0025$ for Eq [11]; $t_{f2} = 0.5$, $t_{d2} = 4$, $\theta_2 = 0.02$ for Eq [12]; and $t_{f3} = 0.5$, $t_{d3} = 5$, $\theta_3 = 0.03$ for Eq [13] and with all other parameters unchanged from (A). Only chemical x is plotted. Chemical y oscillates with the same period as x so it is excluded for clarity. The initial conditions are always $x = y = t = 0$. The parameter $\alpha_i = \theta_i * t_{fi}/t_{di}$ so that the average value of $P_i(t)$ in the pulsate model is equal to the constant term α_i in the vanilla ODE model.

PeerJ PrePrints

1

Figure 1

Numerical integration of Eqs. [1] and [2] with α_1 being replaced by a pulsate function. (A) α_1 is a sine pulse. Initial $x=t=0$, and $y=0.3$. The parameter values are $t_{f1}=1$, $t_{d1}=1$, $\theta_1=0.002$, $\beta_1=0.025$, $K_1=0.5$, $n_1=8$ for Eq. [1] and $\alpha_2=0.0001$, $\beta_2=0.0001$, $K_2=0.5$, $n_2=8$ for Eq. [2]. (B) α_1 is a triangle pulse. Initial $x=t=0$, and $y=0.35$. The parameter values are $t_{f1}=1$, $t_{d1}=1$, $\theta_1=0.0025$, $\beta_1=0.025$, $K_1=0.5$, $n_1=8$ for Eq. [1] and $\alpha_2=0.0001$, $\beta_2=0.0001$, $K_2=0.5$, $n_2=8$ for Eq. [2]. (C) α_1 is a sawtooth pulse. Initial $x=t=0$, and $y=0.25$. The parameter values are $t_{f1}=1$, $t_{d1}=1$, $\theta_1=0.003$, $\beta_1=0.025$, $K_1=0.5$, $n_1=8$ for Eq. [1] and $\alpha_2=0.0002$, $\beta_2=0.0001$, $K_2=0.5$, $n_2=8$ for Eq. [2].

PeerJ PrePrints

PeerJ PrePrints | https://dx.doi.org/10.7287/peerj.preprints.1272v1 | CC-BY 4.0 Open Access | rec: 29 Jul 2015, publ: 29 Jul 2015

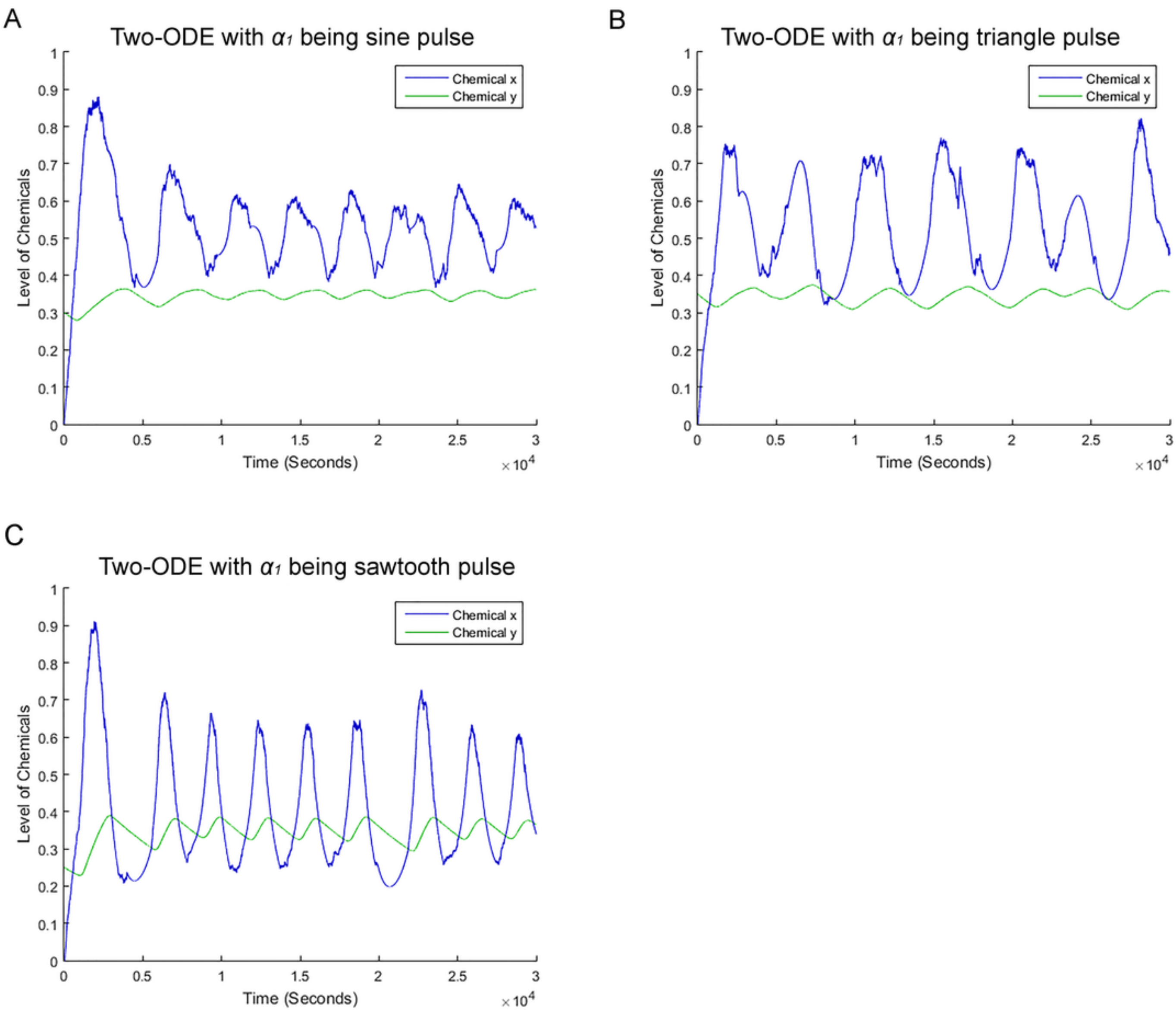

PeerJ PrePrints

PeerJ PrePrints | https://dx.doi.org/10.7287/peerj.preprints.1272v1 | CC-BY 4.0 Open Access | rec: 29 Jul 2015, publ: 29 Jul 2015

2

Figure 2

Numerical integration of Eqs. [1] and [2] with single constant coefficients replaced by pulsate terms. (A) α_1 is replaced by the pulsate function $P_1(t)$. The parameter values are $t_{f1}=0.25$, $t_{d1}=1$, $\theta_1=0.003$, $\beta_1=0.015$, $K_1=0.5$, $n_1=8$ for Eq. [1] and $\alpha_2=0.003$, $\beta_2=0.0001$, $K_2=0.5$, $n_2=8$ for Eq. [2]. (B) α_2 is replaced by the pulsate function $P_2(t)$. The parameter values are $\alpha_1=0.0001$, $\beta_1=0.05$, $K_1=0.5$, $n_1=8$ for Eq. [1] and $t_{f2}=0.25$, $t_{d2}=1$, $\theta_2=0.01$, $\beta_2=0.0001$, $K_2=0.5$, $n_2=8$ for Eq. [2]. (C) β_1 is replaced by the pulsate function $P_1(t)$. The parameter values are $\alpha_1=0.0001$, $t_{f1}=0.25$, $t_{d1}=1$, $\theta_1=0.4$, $K_1=0.5$, $n_1=8$ for Eq. [1] and $\alpha_2=0.011$, $\beta_2=0.0002$, $K_2=0.5$, $n_2=8$ for Eq. [2]. (D) β_2 is replaced by the pulsate function $P_2(t)$. The parameter values are $\alpha_1=0.0001$, $\beta_1=0.01$, $K_1=0.5$, $n_1=8$ for Eq. [1] and $\alpha_2=0.0007$, $t_{f2}=0.25$, $t_{d2}=1$, $\theta_2=0.01$, $K_2=0.5$, $n_2=8$ for Eq. [2]. The initial conditions are always x=y=t=0.

PeerJ PrePrints | https://dx.doi.org/10.7287/peerj.preprints.1272v1 | CC-BY 4.0 Open Access | rec: 29 Jul 2015, publ: 29 Jul 2015

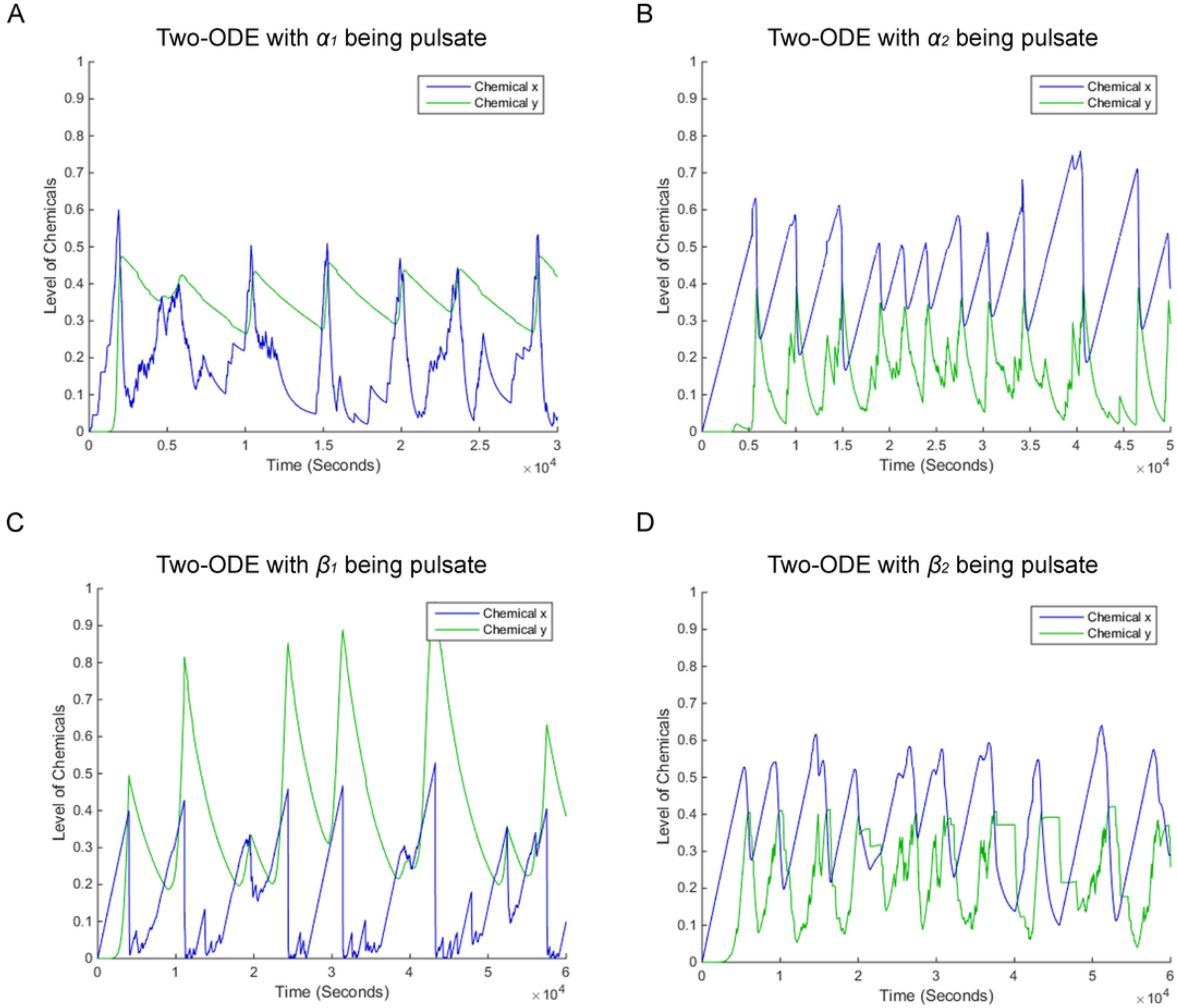

PeerJ PrePrints

3

Figure 3

Numerical integration of Eqs. [1] and [2] with pairs of constant coefficients replaced by pulsate terms. (A) α_1 and β_1 are replaced by the pulsate functions $P_{11}(t)$ and $P_{12}(t)$, respectively. The parameter values are $t_{f11}=0.25$, $t_{d11}=1$, $\theta_{11}=0.001$, $t_{f12}=0.25$, $t_{d12}=1.25$, $\theta_{12}=0.05$, $K_1=0.5$, $n_1=8$ for Eq. [1] and $\alpha_2=0.0003$, $\beta_2=0.0002$, $K_2=0.5$, $n_2=8$ for Eq. [2]. (B) α_1 and β_2 are replaced by the pulsate functions $P_{11}(t)$ and $P_{22}(t)$, respectively. The parameter values are $t_{f11}=0.5$, $t_{d11}=3$, $\theta_{11}=0.0025$, $\beta_1=0.001$, $K_1=0.5$, $n_1=8$ for Eq. [1] and $\alpha_2=0.001$, $t_{f22}=0.5$, $t_{d22}=4$, $\theta_{22}=0.005$, $K_2=0.5$, $n_2=8$ for Eq. [2]. (C) β_1 and α_2 are replaced by the pulsate functions $P_{12}(t)$ and $P_{21}(t)$, respectively. The parameter values are $\alpha_1=0.00005$, $t_{f12}=0.5$, $t_{d12}=3$, $\theta_{12}=0.2$, $K_1=0.5$, $n_1=8$ for Eq. [1] and $t_{f21}=0.5$, $t_{d21}=4$, $\theta_{21}=1$, $\beta_2=0.001$, $K_2=0.5$, $n_2=8$ for Eq. [2]. (D) α_2 and β_2 are replaced by the pulsate functions $P_{21}(t)$ and $P_{22}(t)$, respectively. The parameter values are $\alpha_1=0.0009$, $\beta_1=0.0133$, $K_1=0.5$, $n_1=8$ for Eq. [1] and $t_{f21}=0.5$, $t_{d21}=3$, $\theta_{21}=0.3$, $t_{f22}=0.5$, $t_{d22}=4$, $\theta_{22}=0.02$, $K_2=0.5$, $n_2=8$ for Eq. [2]. (E) α_1 and α_2 are replaced by the pulsate functions $P_{11}(t)$ and $P_{21}(t)$, respectively. The parameter values are $t_{f11}=0.25$, $t_{d11}=1$, $\theta_{11}=0.0003$, $\beta_1=0.0125$, $K_1=0.5$, $n_1=8$ for Eq. [1] and $t_{f21}=0.25$, $t_{d21}=1.25$, $\theta_{21}=0.00125$, $\beta_2=0.000014$, $K_2=0.5$, $n_2=8$ for Eq. [2]. (F) β_1 and β_2 are replaced by the pulsate functions $P_{12}(t)$ and $P_{22}(t)$, respectively. The parameter values are $\alpha_1=0.00007$, $t_{f12}=0.25$, $t_{d12}=1$, $\theta_{12}=0.03$, $K_1=0.5$, $n_1=8$ for Eq. [1] and $\alpha_2=0.00025$, $t_{f22}=0.25$, $t_{d22}=1.25$, $\theta_{22}=0.00015$, $K_2=0.5$, $n_2=8$ for Eq. [2]. The initial conditions are always $x=y=t=0$.

PeerJ PrePrints

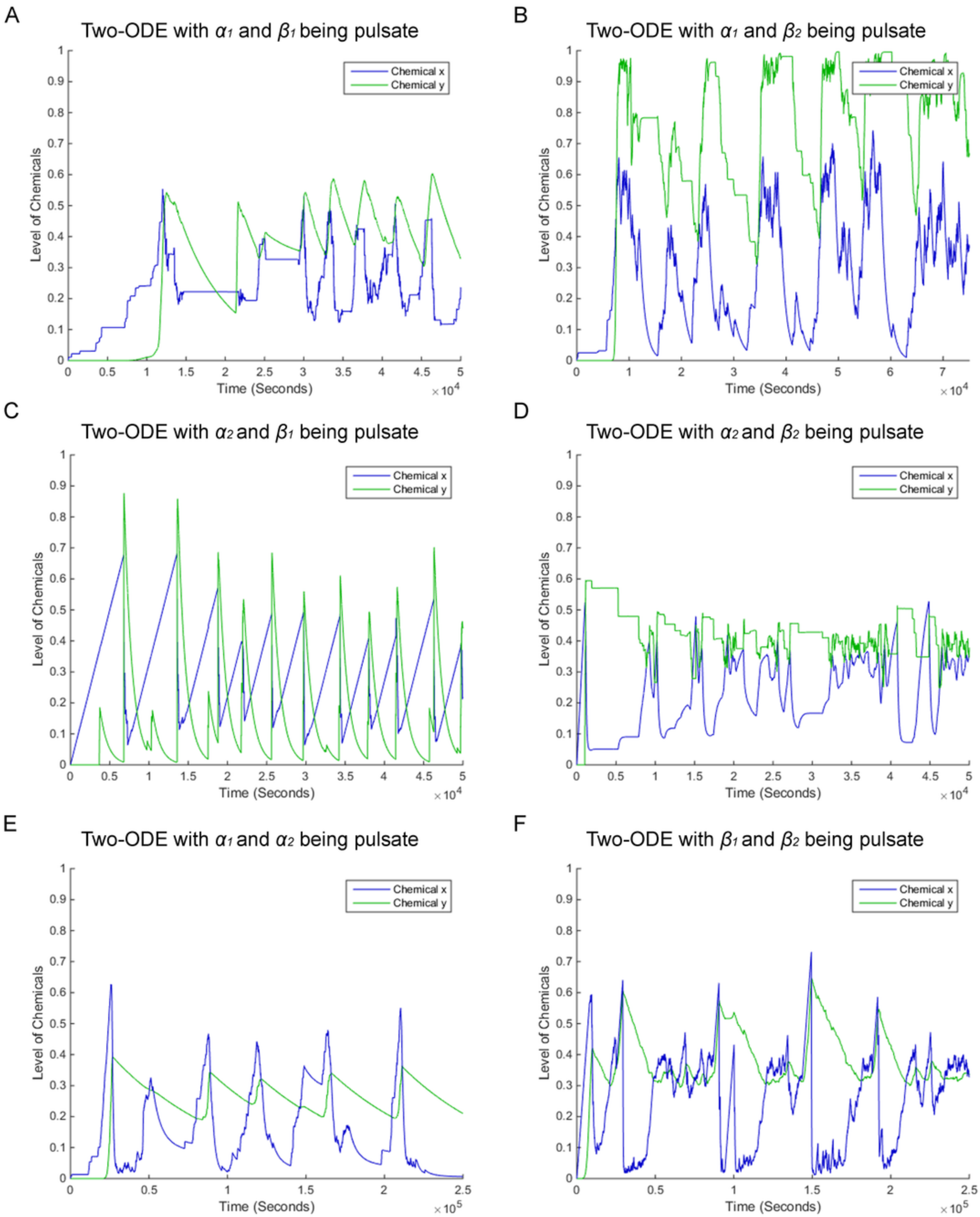

PeerJ PrePrints | https://dx.doi.org/10.7287/peerj.preprints.1272v1 | CC-BY 4.0 Open Access | rec: 29 Jul 2015, publ: 29 Jul 2015

4

Figure 4

Numerical integration of equations [1] and [2] with triples of constant coefficients replaced by pulsate terms. (A) α_1, α_2, and β_2 are replaced by the pulsate functions P_11 (t), P_21 (t), and P_22 (t), respectively. The parameter values are t_f11=0.5, t_d11=3, θ_11=0.005, β_1=0.05, K_1=0.5, n_1=8 for Eq. [1] and t_f21=0.5, t_d21=4, θ_21=0.03, t_f22=0.5, t_d22=4.5, θ_22=0.001, K_2=0.5, n_2=8 for Eq. [2]. (B) α_1, β_1, and α_2 are replaced by the pulsate functions P_11 (t), P_12 (t), and P_21 (t), respectively. The parameter values are t_f11=0.25, t_d11=1, θ_11=0.00005, , t_f12=0.25, t_d12=1.5, θ_12=0.075, K_1=0.5, n_1=8 for Eq. [1] and t_f21=0.25, t_d21=1.25, θ_21=0.001, β_2=0.0002, K_2=0.5, n_2=8 for Eq. [2].

The initial conditions are always x=y=t=0.

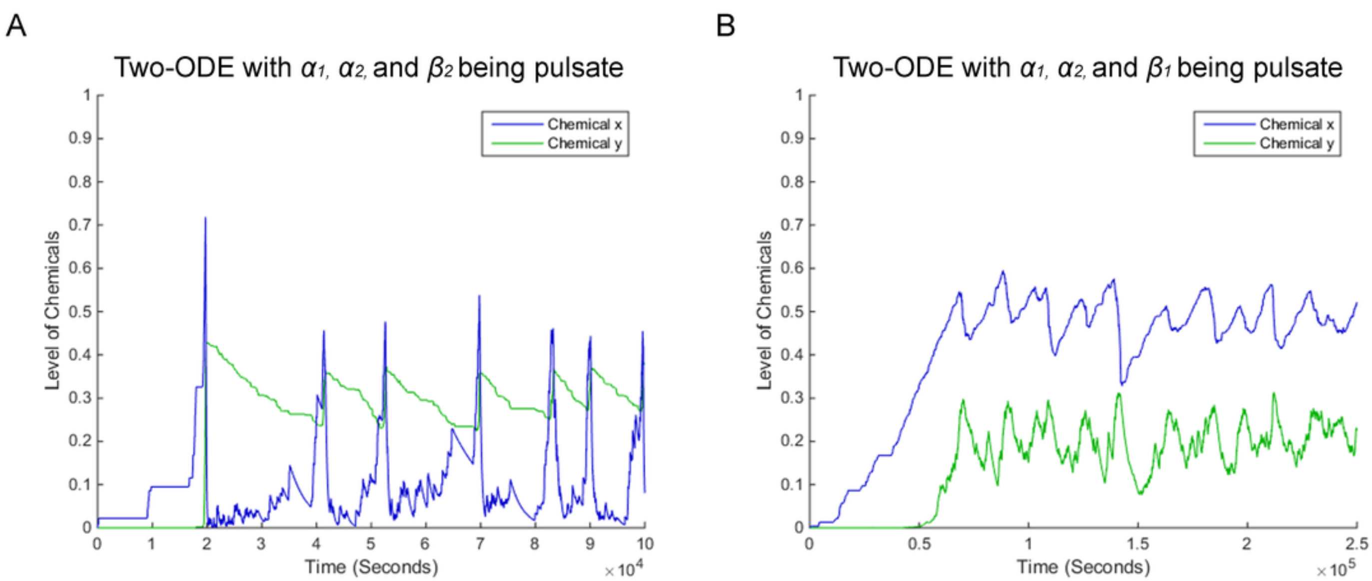

PeerJ PrePrints | https://dx.doi.org/10.7287/peerj.preprints.1272v1 | CC-BY 4.0 Open Access | rec: 29 Jul 2015, publ: 29 Jul 2015

5

Figure 5

A comparison between two-DDE models with varying time lags and two-ODE models with varying pulsate periods. Only chemical x has been plotted. Chemical y oscillates with the same period as x so it is excluded for clarity. (A) Numerical integration of DDE Eqs. [6] and [7] with arbitrarily chosen parameters $\tau_1=250$, $\alpha_1=0.0005$, $\beta_1=0.0125$, $K_1=0.5$, $n_1=8$ for Eq. [6] and $\tau_1=250$, $\alpha_2=3$, $\beta_2=0.02$, $K_2=0.5$, $n_2=8$ for Eq. [7]. (B) Numerical integration of DDE Eqs. [6] and [7] with the same parameters as in (A) except $\tau_1=\tau_2=500$. (C) Numerical integration of ODE Eqs. [1] and [2] where α_1 and α_2 are replaced by the pulsate functions $P_{11}(t)$ and $P_{21}(t)$, respectively. The parameter values are $t_{f11}=0.5$, $t_{d11}=2.5$, $\theta_{11}=0.005$, $\beta_1=0.0125$, $K_1=0.5$, $n_1=8$ for Eq. [1] and $t_{f21}=0.5$, $t_{d21}=2$, $\theta_{21}=0.0175$, $\beta_2=0.0001666667$, $K_2=0.5$, $n_2=8$ for Eq. [2]. (D) Numerical integration of Eqs. [1] and [2] where α_1 and α_2 are replaced by the pulsate functions $P_{11}(t)$ and $P_{21}(t)$, respectively. The parameter values are $t_{f1}=0.5$, $t_{d1}=3$, $\theta_1=0.006$ for Eq. [1] and $t_{f2}=0.5$, $t_{d2}=3.5$, $\theta_2=0.0306$ for Eq. [2]. All other parameters are the same as in (C). The initial conditions are always x=y=t=0. The parameter $\theta_i^{long}=\theta_i^{short}*t_d^{long}/t_d^{short}$ so that the average values of $P_i(t)$ in the long-period ODE pulsate model and the short-period ODE pulsate model are equal.

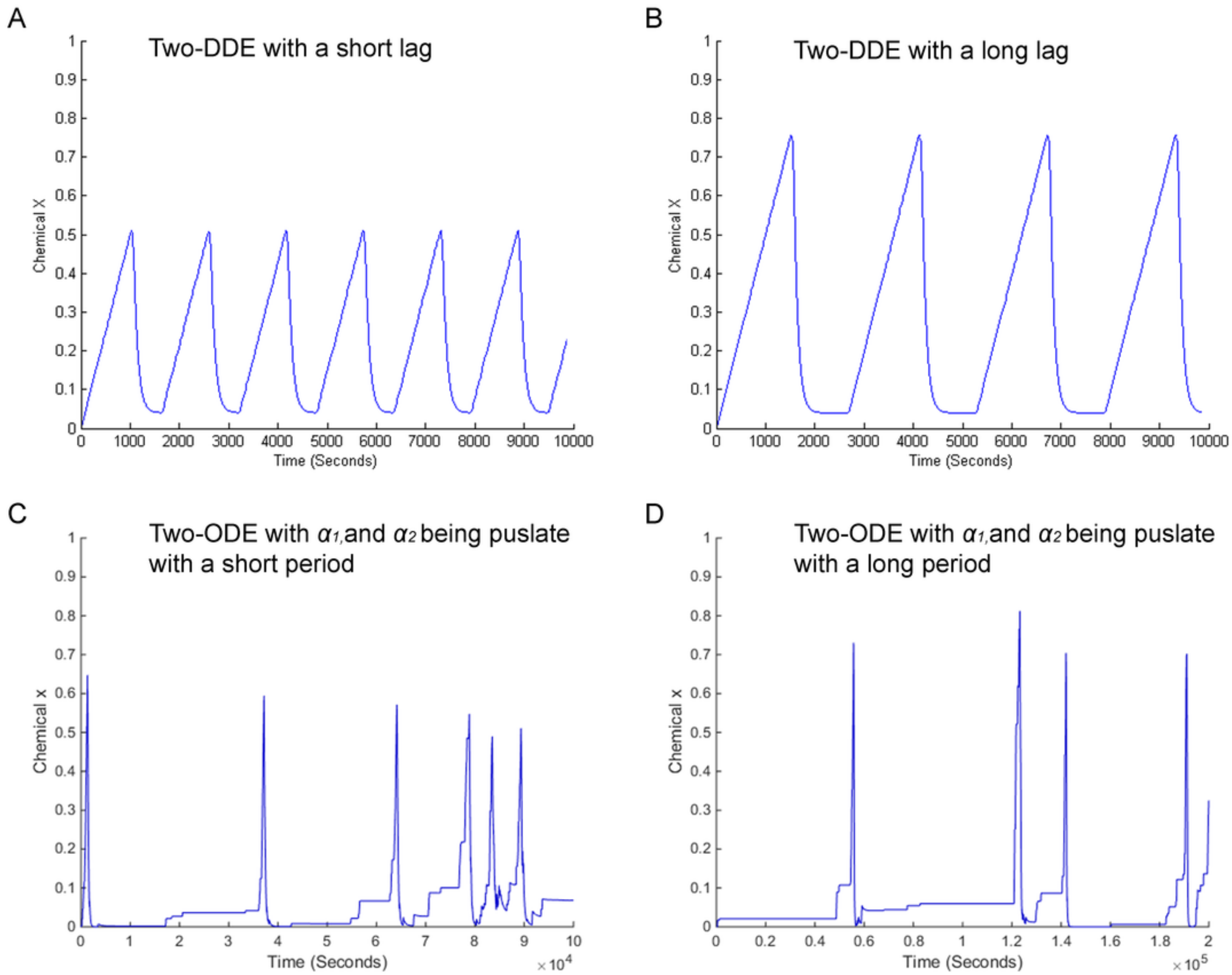

PeerJ PrePrints

6

Figure 6

A comparison between three-ODE models, three-DDE models, and three-ODE models with varying pulsate periods. (A) Numerical integration of the standard three-ODE model, Eqs. [8-10], with arbitrarily chosen parameters $\alpha_1=0.0004166666667$, $\beta_1=0.0125$, $K_1=0.5$, $n_1=8$ for Eq. [8]; $\alpha_2=0.0025$, $\beta_2=0.0001666667$, $K_2=0.5$, $n_2=8$ for Eq. [9]; and $\alpha_3=0.003$, $\beta_3=0.0001666667$, $K_3=0.5$, $n_3=8$ for Eq. [10]. (B) Numerical integration of the three-ODE model, Eqs. [11-13], with arbitrarily chosen parameters $t_{f1}=0.25$, $t_{d1}=1$, $\theta_1=0.0017$ for Eq. [11]; $t_{f2}=0.25$, $t_{d2}=1.25$, $\theta_2=0.0125$ for Eq. [12]; and $t_{f3}=0.25$, $t_{d3}=1.5$, $\theta_3=0.018$ for Eq. [13] and with all other parameters unchanged from (A). (C) Numerical integration of the three-DDE model, Eqs. [14-16]. All parameters are the same as in (A) except $\tau_1=\tau_2=\tau_3=300$. (D) Numerical integration of the three-ODE model, Eqs. [11-13] with arbitrarily chosen parameters $t_{f1}=0.5$, $t_{d1}=3$, $\theta_1=0.0025$ for Eq [11]; $t_{f2}=0.5$, $t_{d2}=4$, $\theta_2=0.02$ for Eq [12]; and $t_{f3}=0.5$, $t_{d3}=5$, $\theta_3=0.03$ for Eq [13] and with all other parameters unchanged from (A). Only chemical x is plotted. Chemical y oscillates with the same period as x so it is excluded for clarity. The initial conditions are always x=y=t=0. The parameter $\alpha_i=\theta_i*t_{fi}/t_{di}$ so that the average value of $P_i(t)$ in the pulsate model is equal to the constant term α_i in the vanilla ODE model.

PeerJ PrePrints

PeerJ PrePrints | https://dx.doi.org/10.7287/peerj.preprints.1272v1 | CC-BY 4.0 Open Access | rec: 29 Jul 2015, publ: 29 Jul 2015

PeerJ PrePrints